Advances in Water Resources 32 (2009) 1297–1310

Contents lists available at ScienceDirect

Advances in Water Resources

journal homepage: www.elsevier.com/locate/advwatres

What indicators can capture runoff-relevant connectivity properties of the micro-topography at the plot scale?

Michael Antoine *, Mathieu Javaux, Charles Bielders

Department of Environmental Sciences and Land Use Planning, Université Catholique de Louvain (UCL), Croix du Sud, 2, bte 2, B-1348 Louvain-la-Neuve, Belgium

ARTICLE INFO

Article history:
Received 19 December 2008
Received in revised form 6 May 2009
Accepted 9 May 2009
Available online 18 May 2009

Keywords:
Connectivity
Indicator
Micro-topography
Surface storage
Runoff modelling
Plot scale
Numerical experiments

ABSTRACT

Although connectivity is acknowledged as a key factor of a catchment hydrological behaviour, it still misses reference evaluation methodologies. Therefore the objective of the paper is to evaluate different quantitative indicators of hydrological connectivity, using the concepts of structural and functional connectivity commonly used in ecology. The indicators were tested on contrasted numerical fields of micro-topography that present distinct hydrological responses.

The investigated structural connectivity indicators, mostly used so far in porous or fractured media, were the semivariogram, the bivariate entropy integral scale, the *n*-point rectilinear connectivity integral scale, the connectivity function integral scale, the percolation threshold and the Euler number. The first three indicators were not able to discriminate between the three extreme types of micro-topographical fields whereas the last three indicators were successful. However, relating the latter three indicators to the hydrological response of a topographical field appears uncertain. We therefore proposed a functional connectivity indicator by adapting the 'volume to breakthrough' concept: the degree of surface connection as a function of the surface storage filling. This indicator was capable of discriminating between the micro-topographical types. It could be used to conceptualize the process of depression filling and therefore may become an effective characteristic of an elementary representative area in large scale hydrologic model.

1. Introduction

The word 'connectivity' has been used in a variety of disciplines, such as neurological sciences, mathematical graph theory, computer and communications technologies, meta-population biology, landscape ecology, hydrology and geomorphology. The connectivity concept has been developed to investigate the influence of the intrinsic organization of heterogeneities on the global behaviour of the system that contains those heterogeneities. It is an essential factor to take into account when modelling heterogeneous systems.

In the context of landscape ecology, the study of connectivity is an old concern. The original definition of landscape connectivity is *the degree to which the landscape facilitates or impedes movement between resource patches* [45]. It combines the effect of the landscape structures as well as the species ability to move in this landscape and the associated risk [46]. Hence landscape connectivity integrates two characteristics: the physical patterns in the landscape and the behavioural processes of the species in interaction with those patterns [10]. Therefore landscape connectivity can be divided into two sub-concepts: the structural and the functional connectivity. Structural connectivity aims at describing the physical links among habitat patches and are measurable by spatial metrics whereas functional connectivity accounts for the flow of organisms through the landscape, which is species specific and may dependent on broader-scale influences (i.e., the wind direction, the water currents) [44].

In the context of subsurface hydrology, the study of connectivity has been specifically dedicated to the water fluxes per-se (to determine solute transport subsequently) in the vadose zone and in fractured media. Connectivity of the soil matrix (or preferential flow paths, high-K flow paths) typically refers to the presence of continuous fast flow streamlines of water and/or solutes transport [29] or, on the contrary, to the presence of cut off structures that obstruct the flow [7,23,31]. It is implicitly assumed to be a purely statistical concept [13,48] associated with the geometry of the pore space [28] or the fractures [52]. This approach of the connectivity concept is mostly structural (in the sense defined in landscape ecology) as it is based on geometrical properties, although the extraction of the flow network out of the pore system is first of all based on a movement criterion (the local hydraulic conductivity needs to be high, or implicitly the pore radius needs to be large).

Hydrological connectivity, especially in the field of surface hydrology, still misses of a widely accepted definition [5] as its meaning varies from author to author, depending on the context

* Corresponding author. Tel.: +32 (0)10 47 38 27; fax: +32 (0)10 47 38 33.
E-mail address: michael.antoine@uclouvain.be (M. Antoine).

0309-1708/$ - see front matter © 2009 Elsevier Ltd. All rights reserved.
doi:10.1016/j.advwatres.2009.05.006

and the sources of information that are used to characterize it (see [5] for an in-depth review of the concept of hydrological connectivity). Because water flow is not easily observable by direct methods at every location in a landscape, hydrological connectivity has been studied through a variety of mostly indirect approaches, including the study of observable patterns [6], terrain indexes derived from surface topography [19,21], or potential water movement in the system combining topographical and land use information and modelling [21,39,12]. If one refers to the connectivity concept used in ecology, then the connectivity derived from terrain information is of the 'structural' type whereas the connectivity derived from a combination of modelling and geographical information is of the 'functional' type. The study of observable patterns, such as vegetation patterns [25], rill, gully and river networks [15], soil moisture patterns [51], may at first appear to be related to the structural connectivity concept, yet these footprints of water flow actually carry information regarding both the spatial continuity of the water (structural connectivity) as well as the amount of water and/or the discharge rate passing at different locations (functional connectivity). Hence, depending on the approach, hydrological studies highlight the structural connectivity, functional connectivity, or some partial combination of both concepts.

In order to promote progress in the study of hydrological connectivity, it seems essential to settle on a common, precise definition. It is suggested here to make use of the connectivity concept employed in ecology as it has been applied successfully for a long time by a large scientific community, albeit in a different scientific domain. The conceptual definition of connectivity that will be used here is thus the *structural and/or functional continuity between elementary unit or subset of elementary units encompassed in a larger space*. *Structural* connectivity refers to continuum properties of state variables (such as altitude or soil surface properties) in space, whereas *functional* connectivity is process-based and reflects the capacity (or the rate of transfer) of water (and associated particles or molecules) to move in the system in response to a boundary stimulus. Let us note that [5] speak of static and dynamic connectivity to distinguish between structural and functional connectivity. However, we prefer the term 'structural connectivity' over 'static connectivity', as structural connectivity is not necessarily a static property, i.e., surface topography can be temporally highly dynamic, especially at small scales. The term static may therefore be misleading.

It is apparent from the above definition that both structural and functional connectivity may be scale-dependent [9]. Both concepts may also depend on the history of flows through the system, as these flows are capable of modifying the surface topography and the network of other landscape elements that may affect surface flow (e.g., land use, vegetation). In addition, as opposed to structural connectivity, functional connectivity will be directly dependent on the boundary conditions of the system. Indeed, the functional connectivity is revealed in the hydrological response of a surface to a stimulus applied at the boundary of the system. The promptness of the system to react to a modification of the boundary condition is a measure of functional connectivity (in the sense defined in landscape ecology, where the species are replaced by water molecules or solutes), such as an early arrival time in a breakthrough experiment for instance [29] or a high value of effective transmissivity in pumping test. Hence, whereas hydrological structural connectivity may be studied without specifying the boundary conditions, the characterization of functional connectivity cannot be dissociated from the boundary conditions.

In order to evaluate quantitatively the structural and the functional connectivity of an hydrological system, several indicators have been used. For [20], semivariograms are useful in a primary step to determine the appropriate scale at which patterns must be investigated. Nevertheless Western et al. [50] state that semivariograms are better at describing continuity than connectivity. Indeed, in their study, connected and random patterns of soil water content were not distinguished by traditional geostatistics. It is due to the assumption that relations between points depend only on their Euclidian distance, although it is most of all the presence of connecting paths that determines the connectivity, whatever their shapes [50]. In a parallel context, Knudby and Carrera [28] found that 2-points statistics, including the semivariogram and the bivariate entropy, were inadequate to account for the structural connectivity impact on water and solute transport. On the other hand, multiple-point statistics, such as the connectivity function of Allard and HERESIM-Group [2], performed yet better [28]. With this function, Western et al. [51] could also discriminate between spatial patterns exhibiting contrasted structural connectivity characteristics, and relate it to different hydrologic behaviours. Topological properties of the structures, such as the Euler number, may be used to quantify the connectivity properties, and may constraint the construction of realistic numerical fields [49]. When cut off structures (terraces and dams for Bellin et al. [3], vegetation bands for Imeson and Prinsen [25]) or impermeable interfaces [34] obstruct the flows, the ratio between the actual connections (limited by the obstructing elements) and the potential connections (if the obstructing elements where missing) is a straightforwards measurement of structural connectivity. In subsurface hydrology, Scheibe [41] proposed that breakthrough curves may provide functional indicators of connectivity, as the way high or low conductivity regions were patterned were reflected in the arithmetic mean velocity and the early and late arrival times. And indeed, the functional connectivity indicators that were based on the information provided by the breakthrough curve performed the best for Knudby and Carrera [28]. In a global context, Bracken and Croke [5] put the *volume to breakthrough* forward as an unifying concept in quantifying the functional connectivity at a range of spatial scale.

Because it is independent of boundary conditions, the characterization of structural connectivity appears more straightforward than functional connectivity. Yet it is functional connectivity that best reflects the hydrological behaviour of a given surface. Clearly, functional connectivity must to some extent be dependent on structural connectivity, as pattern and process are often assumed to be linked [20], but the nature of this relationship is largely unknown. It is therefore of interest to investigate whether structural connectivity indicators can be used to assess the functional connectivity for specific boundary conditions. Therefore, the general objective of this study is to test and compare different quantitative indicators of both structural and functional connectivity and to evaluate their robustness in relation to particular hydrologic behaviour. Our specific objectives are (1) to show that the structural connectivity of the micro-topography affects the runoff production, (2) to assess the discriminative capacity of previously defined indicators of structural connectivity with regard to distinct hydrologic behaviours and (3) to derive a simple functional connectivity indicator for surface hydrology.

We will focus our analysis on small bare plots that have similar dimension as the dimension of the numerical gridcell of spatially distributed hydrological hillslope models (i.e., $\sim m^2$). This choice is driven by several reasons. (1) Methods exist to characterize in great detail the soil micro-topography at the square meter scale, which can be used to derive structural connectivity indicators; (2) characterizing the hydrological response at such scales is fairly straightforward, thereby allowing to characterize the functional connectivity. This makes it possible to study in detail the relationship between structural and functional connectivity. (3) Besides these practical considerations, it is of particular relevance to derive such a relationship at the square meter scale. Indeed, one can never hope to resolve field, hillslope or watershed-scale hydrological models with millimeter scale resolution, for obvious computa-

tional (and data acquisition) reasons. The challenge is therefore to integrate in current modelling approaches the hydrological response at the sub-cell scale by integrating information about the connectivity. Connectivity statistics could provide parameters of the subgrid variability in large scale models [51] as it is in fact the connectivity inside every grid cell that controls the evolution of the effective drainage areas, which is a main factor for the non-linear catchment response.

As a first approach, we will simplify the problem by not considering any infiltration, which is left for future studies. At that scale, we hypothesize that rainfall is spatially uniform. Various potential indicators of connectivity are described in Section 2. Some of these require a complete knowledge of the micro-topography. Therefore our study is based on numerical experiments, which meet more easily this requirement. To evaluate the potential of the different indicators, we investigated their discriminative capacity on extreme topographical cases. We chose the method of Zinn and Harvey [53] to generate the extreme cases of micro-topography.

2. Material and methods

2.1. Structural connectivity indicators derived from point to point analysis

The structural connectivity indicators are applied on the topographical fields in the absence of any trend (the macroscopic slope is subtracted), so it is only the effect of the local micro-topography that is taken into account.

2.1.1. Methods applicable to continuous fields

2.1.1.1. Semivariogram. The semivariogram γ describes the degree of spatial dependence of a random field $Z(\mathbf{x})$, with $\mathbf{x}$ a position vector in the spatial domain D. For a distance vector $\mathbf{d}$:

$$\gamma(\mathbf{d}) = \frac{1}{2} Var[Z(\mathbf{x}) - Z(\mathbf{x}+\mathbf{d})] \quad \forall \mathbf{x} \in D \tag{1}$$

It is used in the context of connectivity by, among others, Western et al. [51].

2.1.1.2. Entropy. Entropy is a measure of disorder, while connectivity implies order. Therefore, entropy of a connected field may be smaller than for an unconnected field [28]. If $f_d(\zeta,\zeta')$ is the stationary bivariate probability density function (PDF) of the random variables $\zeta = Z(\mathbf{x})$ and $\zeta' = Z(\mathbf{x}+\mathbf{d})$, separated by a distance vector $\mathbf{d}$, then the entropy $H_f(\mathbf{d})$ of the distribution $f_d(\zeta,\zeta')$ is defined by:

$$H_f(\mathbf{d}) = -\int_{-\infty}^{\infty}\int_{-\infty}^{\infty} (\ln f_d(\zeta,\zeta')) f_d(\zeta,\zeta') \partial\zeta\, \partial\zeta' \tag{2}$$

Since the functions $\ln f_d(\zeta,\zeta')$ and $f_d(\zeta,\zeta')$ increase together, couple combinations with low probabilities will increase the entropy value [26]. This occurs when the number of distinct combinations of couple increases. Thus the higher the disorder, the higher the entropy (this will be the case for instance if couple combinations follow a uniform bivariate distribution). A discrete approximation to this distribution can be computed by distributing the value of each random variable among K categories (intervals of values) and by computing the following equation [26]:

$$H_f(\mathbf{d}) = -\sum_{k=1}^{K}\sum_{k'=1}^{K} (\ln p_{k,k'}(\mathbf{d})) p_{k,k'}(\mathbf{d}) \tag{3a}$$

$$p_{k,k'}(\mathbf{d}) = \text{Prob}\{Z(\mathbf{x}) \in \text{category } k,\ Z(\mathbf{x}+\mathbf{d}) \in \text{category } k'\} \tag{3b}$$

The relative bivariate entropy $H_r(\mathbf{d})$ is defined by:

$$H_r(\mathbf{d}) = \frac{H_f(\mathbf{d}) - H_f(0)}{H_f(0)} \tag{4a}$$

$$H_f(0) = -\sum_{k=1}^{K} (\ln p_k) p_k \tag{4b}$$

$H_r(\mathbf{d})$ varies between 0 and 1. $H_r = 1$ means a maximum entropy and corresponds to the case of two independent variables.

2.1.2. Methods applicable to binary fields

2.1.2.1. Binarization by threshold. Methods described hereafter require binary fields (fields of 0 and 1). Given a field Z composed of multiple pixels, it can be divided into two subsets of pixels S and S^C labeled 0 and 1, so that $Z = S \bigcup S^C$ (Z is thus completely defined by a binary field). Depending on the subset of interest, S or S^C is used to compute the connectivity indicators. The rules used for dividing the field into two depend on the context. A common way is to attribute a pixel $\mathbf{x}$ to S or S^C depending on whether its value $Z(\mathbf{x})$ is above or below a threshold value z [37,40,28,51]. We will consider that the threshold value z accounts for the mean absolute water level. Every pixel whose height is under that level is submerged by water and thus is considered as being part of the runoff pathways and receive a value 1

$$I_{th}(\mathbf{x};z) = \begin{cases} 1 & \text{if } Z(\mathbf{x}) \leqslant z \\ 0 & \text{else} \end{cases} \tag{5}$$

This procedure presents some limitation as we will explain in the next paragraph. Although it is the only one that generates comprehensive binary fields for the Euler number. Therefore, this binarization process I_{th} will be used to compute the Euler number in function of z. The field of interest is in that case the subset of pixels whose elevation is below the threshold value z ($I_{th} = 1$, Eq. (5)).

2.1.2.2. Binarization by watershed procedure. Because the level of a pixel can be above a certain threshold yet its water may (in some cases) or may not (in other cases) flows up to the outlet, we tested an other binarization procedure than the common threshold-based one. It is based on the delineation of the area hydrologically connected to the downstream boundary of the field (i.e., a watershed delineation for which the outlet is made of all the pixels at the downstream boundary). We raise step by step a mean horizontal level of water z [m] that submerges gradually the micro-topography. For each step, the topography is modified by considering, in every point, the maximum altitude between the original soil surface height and the absolute submerging level z. This incrementally updated topography is considered for the watershed delineation corresponding to the submerging level z. The binarization procedure attributes to every pixel a value of 1 or 0 depending on whether it is part or not of the updated watershed corresponding to the z value. As surface depressions are progressively submerged by the fictive water level z, more and more surface becomes part of the watershed related to the downstream boundary

$$I_{ws}(\mathbf{x};z) = \begin{cases} 1 & \text{if } \max(Z(\mathbf{x}),z) \in \text{watershed of the downstream} \\ & \quad \text{boundary of the field} \\ 0 & \text{else} \end{cases} \tag{6}$$

2.1.2.3. n-Point rectilinear connectivity integral scale. n-Point rectilinear connectivity is the probability that pixels at n locations located along a linear path are all in the field of interest (in our case $I_{ws} = 1$). Given $\mathbf{u}$ a unit vector in a specific direction (in our case $\mathbf{u}$ has the size of one pixel and is oriented upslope along the macroscopic mean slope that was previously subtracted for the analysis) and given a height threshold z, the n-point connectivity $K(\mathbf{u};n;z)$ is:

$$K(\mathbf{u};n;z) = \mathrm{Prob}\{I_{ws}(\mathbf{x};z)=1, I_{ws}(\mathbf{x}+\mathbf{u};z) = 1,\ldots,I_{ws}(\mathbf{x}+n\mathbf{u};z)=1\} \quad (7a)$$

$$= E[I_{ws}(\mathbf{x};z)I_{ws}(\mathbf{x}+\mathbf{u};z)\ldots I_{ws}(\mathbf{x}+n\mathbf{u};z)] \quad (7b)$$

$$= E\left\{\prod_{j=1}^{n} I_{ws}[\mathbf{x}+(j-1)\mathbf{u};z]\right\} \quad (7c)$$

where $\mathbf{x}, \mathbf{x}+\mathbf{u}, \mathbf{x}+2\mathbf{u}, \ldots, \mathbf{x}+n\mathbf{u}$ are the locations at which the binary indicator variable I_{ws} is evaluated. $K(\mathbf{u};n;z)$ gives the probability of observing a continuous string of n points in the field of interest. We can then compute the n-point rectilinear connectivity integral scale which corresponds to the mean length L_K [m] of the continuous string:

$$L_K = pixel\_length \int_0^{n\_max} K(\mathbf{u};n;z)\partial n \quad (8)$$

where *n_max* is the maximum number of pixels in the field along the direction considered. This indicator measures only straight rectilinear connectivity; any undulation would break that connectivity and reduce L_K [30]. We computed this indicator at the outlet side of the field following the mean slope direction that has been subtracted. This means that the linear features taken into account are parallel to the macroscopic slope and are connected at one end to the downstream boundary.

2.1.2.4. Connectivity function integral scale. The connectivity function defined by Allard and HERESIM-group [2] has been used among others by Western et al. [51], Pardo-Iguzquiza and Dowd [38], Knudby and Carrera [28], Xu et al. [52]. Given a point located at $\mathbf{x}$, and another point located at $\mathbf{x}+\mathbf{d}$ separated from the first by a direct distance $\mathbf{d}$ and belonging to the same subset ($I_{ws}=1$ in our case), those points are said to be connected ($\mathbf{x} \Longleftrightarrow \mathbf{x}+\mathbf{d}$) if they can be joined by a path whose points are in their subset. The connectivity function $\tau(\mathbf{d},z)$ expresses the probability that two points of the subset of interest separated by a direct distance $\mathbf{d}$ are linked by pixels of their subset:

$$\tau(\mathbf{d},z) = P(\mathbf{x} \Longleftrightarrow \mathbf{x}+\mathbf{d}, I_{ws}(\mathbf{x}+\mathbf{d};z)=1 | I_{ws}(\mathbf{x};z)=1) \quad (9)$$

$\tau(\mathbf{d},z)$ is the same as $K(\mathbf{u};n=\mathbf{d}/pixels_{size};z)$ if computed in one single direction. The connectivity function integral scale L_τ [m] represents the average distance over which pixels are connected and can be computed by:

$$L_\tau(z) = \int_0^\infty \tau(\mathbf{d},z)\partial\mathbf{d} \quad (10)$$

2.1.2.5. Percolation. Percolation theory considers that a medium is connected if a continuous path exists between opposite boundaries. The percolation threshold is the threshold value for the binarization procedure that generates a cluster in the subset of interest that spans the entire domain and connects boundaries in case the domain is finite. If the domain is infinite, in some specific cases (for instance when the field is discretized on a square grid and when the values are set at random in the field), a theoretical value for the percolation threshold exists [24,31]. If the domain is finite, border effects occur and the percolation threshold is expressed by a probability. In our case, the field of interest is determined by watershed delineation. Values of the pixels are not set at random and therefore the value of the threshold is not in accordance with classical percolation theory. Consequently, our percolation function provides only the observed probabilities that the watershed connected to the downstream boundary of the field reaches at least one pixel of the upstream boundary.

2.1.2.6. Euler number. The Euler number χ (or Euler characteristics, Euler–Poincaré characteristics) is defined for 2D binary shapes as (Eq. (11)) the number of isolated objects N (close convex) minus the number of holes G (closed concave). G is equivalent to the number of redundant connections (a redundant connection can be cut without creating an additional isolated component). According to Euler's formula, χ can be calculated by the number of nodes minus the number of bonds. In case the structure is partitioned into convex volume elements each defined by a number of vertices, edges and faces, the Euler number may be calculated for 2D grids by $\#vertices - \#edges + \#faces$. The Euler characteristics reported to the volume of investigation is called the volumetric Euler characteristic, and was used to characterize the connectivity of pore space and cracks [48,49]

$$\chi(z) = N(I_{th}(z)=1) - G(I_{th}(z)=1) \quad (11)$$

2.2. Functional connectivity indicator: simplified hydrograph and surface storage dynamics

When the soil infiltration rate is lower than the rainfall intensity, water starts to accumulate at the surface. Puddles progressively overflow and water either accumulates in adjacent depressions, or flows to the downstream boundary, initiating runoff [12]. As the ponded water layer thickness increases, larger part of the plot that produces local runoff connects to the downstream boundary and consequently the global runoff coefficient of the field increases. To account for the effect of the micro-topography on the initiation of runoff, a cellular automaton model was used. It is a simple filling algorithm where the velocity of the water is considered infinite. Given a rainfall intensity I [m/s], for a field of surface S [m^2] during a specific time interval Δt [s], a small volume of water $\Delta V = SI\Delta t$ [m^3] is uniformly distributed on the surface of the plot. The water volume by pixel $\Delta V_{i,j}$ is equal to $\Delta V/\#pixels$. Each $\Delta V_{i,j}$ moves immediately to the lowest point it can reach following the steepest absolute water level gradient (soil level + water thickness) computed in a 8-neighbors scheme. $\Delta V_{i,j}$ is eventually added to previous accumulated water in the depression and increases the water thickness at that point. If the depression overflows, the excess water flows further. When the lowest point reached by the water is situated at the downstream boundary, the water is taken out of the field and is summed up in the simplified hydrograph. After all the $\Delta V_{i,j}$ have been redistributed, the time is increased by Δt. This method is similar to the one of Darboux et al. [12] except that these authors start by randomly distributing the water. The computation principle is illustrated in Fig. 1.

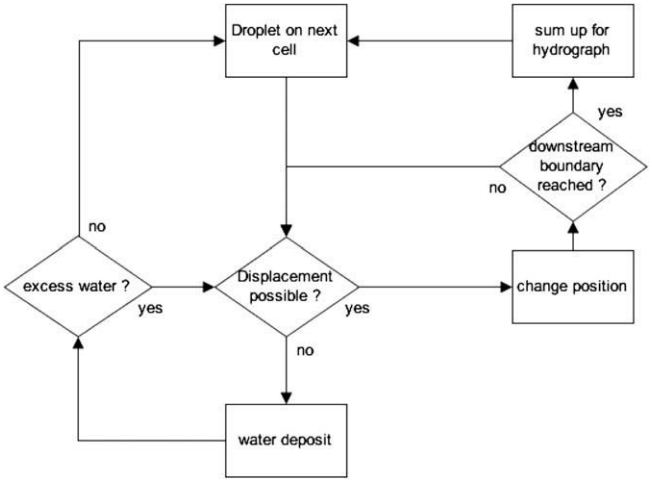

Fig. 1. Flowchart of the filling algorithm to compute the simplified hydrograph.

The method produces simplified hydrographs as it does not take explicitly into account the transfer time of water inside the field, i.e., the water velocity is infinite. As a result, the live storage zone (the dead storage zone is defined as the volume in a reservoir below the lowest controllable level and corresponds to the surface retention; live storage zone is the water above that level and corresponds to the surface detention) is null. In summary, these simplified hydrographs are the results of a simple filling algorithm that is fast to compute and they only show the effect of the water storage in the depressions (dead storage zone) on runoff triggering, under the hypothesis that surface storage is empty at the beginning of the experiment.

These simplified hydrographs can be scaled when we express the runoff coefficient C (instantaneous outflow/instantaneous inflow [$m^3\ s^{-1}/m^3\ s^{-1}$]) as a function of the cumulated inflow [m^3]. Since no infiltration and time transfer were considered in the model, and since the rain is uniform, C is equivalent to the ratio of area connected to the downstream boundary to the total surface of the topographical field [m^2/m^2]. The runoff coefficient C will vary between 0 and 1 when the full surface will be connected to the outflow boundary. The area under the curve C in function of the cumulated inflow is equal to the total volume of runoff [m^3]. The area between 1 and the curve C in function of the cumulated inflow corresponds to the actual dead storage [m^3]. We can thus express the ratio of surface connected to total surface as a function of the water stored in the depressions of the field. We will call this indicator the relative surface connection function. It describes the dynamical effect of the surface storage and it may serve as an indicator for surface functional connectivity. This is illustrated in Fig. 2.

2.3. Runoff model

In order to study the impact of the micro-topography patterns on the runoff and both the live and dead storages, we developed a small scale hydraulic model that simulates the runoff flow and the resulting hydrographs given the micro-topography and the rain intensity. Overland flow can be described by the depth-averaged unsteady flow equations commonly referred to as the shallow flow equations or Saint-Venant equations [14]. If computed in 1D along the x-axis, the equation of momentum is expressed by:

$$\frac{1}{g}\frac{\partial \bar{v}_x}{\partial t}+\frac{\bar{v}_x}{g}\frac{\partial \bar{v}_x}{\partial x}+\frac{\partial h}{\partial x}+\frac{\partial z}{\partial x}+\frac{\partial h_r}{\partial x}=0 \tag{12}$$

where g is the gravity acceleration [m/s^2], $\bar{v}_x$ the depth-averaged velocity [m/s], h the water layer thickness [m], z the soil level [m] and $\frac{\partial h_r}{\partial x}$ the friction slope [–]. Due to the complexity of the topographies (high local gradient of altitude and high divergence of that gradient), the application of the full equation to our scenarios results in numerical problems (oscillations). We were forced to decrease the equation complexity by using the diffusive wave form of the Saint-Venant equation which is expressed by:

$$\frac{\partial h}{\partial x}+\frac{\partial z}{\partial x}+\frac{\partial h_r}{\partial x}=0 \tag{13}$$

In this simplified equation, both the local acceleration term $\left(\frac{1}{g}\frac{\partial \bar{v}_x}{\partial t}\right)$ and the convective term $\left(\frac{\bar{v}_x}{g}\frac{\partial \bar{v}_x}{\partial x}\right)$ are neglected. Backwater effects are only reflected in the pressure term $\left(\frac{\partial h}{\partial x}\right)$ and no hydraulic jump can be modeled. This equation is normally used for permanent and non-uniform regime. Time is discretized in time steps in which the steady state is thus assumed. We used the Darcy–Weisbach formula for the friction head

$$\frac{\partial h_r}{\partial x}=\lambda\frac{1}{4R_h}\frac{\bar{v}_x^2}{2g} \tag{14}$$

where λ [–] is the Darcy–Weisbach friction factor and R_h [m] is the hydraulic radius that is equal to $\bar{h}$ the mean local water depth on the small interval ∂x. By combining Eqs. (13) and (14) we can find a relation between the velocity and the gradient of absolute water level

$$\bar{v}_x=\sqrt{-\frac{8g\bar{h}}{\lambda}\frac{\partial(h+z)}{\partial x}} \tag{15}$$

For laminar flow, the Reynolds number $Re=\frac{\bar{v}D}{\nu}=\frac{\bar{v}4R_h}{\nu}=\frac{\bar{v}4\bar{h}}{\nu}\leqslant 2000$, where D is the characteristic length [m] and the denominator ν is the kinematic viscosity [m^2/s]. In that case the friction factor was determined by [11]:

$$\lambda=\frac{C_L}{Re} \tag{16}$$

where C_L is a constant that is equal to 96 for a smooth surface and is larger if the surface is rough. For turbulent flow ($Re\geqslant 2000$), the friction factor was determined by [22]:

$$\frac{1}{\sqrt{\lambda}}=-2\log_{10}\left(\frac{\varepsilon}{3}+\frac{2.5}{Re\sqrt{\lambda}}\right) \tag{17}$$

with ε the relative roughness [–]

$$\varepsilon=\frac{k_s}{4\bar{h}} \tag{18}$$

where k_s [m] is the diameter of soil particles that produce the surface roughness.

The algorithm is implemented in space using a de-centered grid (Fig. 3) for the velocities that are computed independently in the

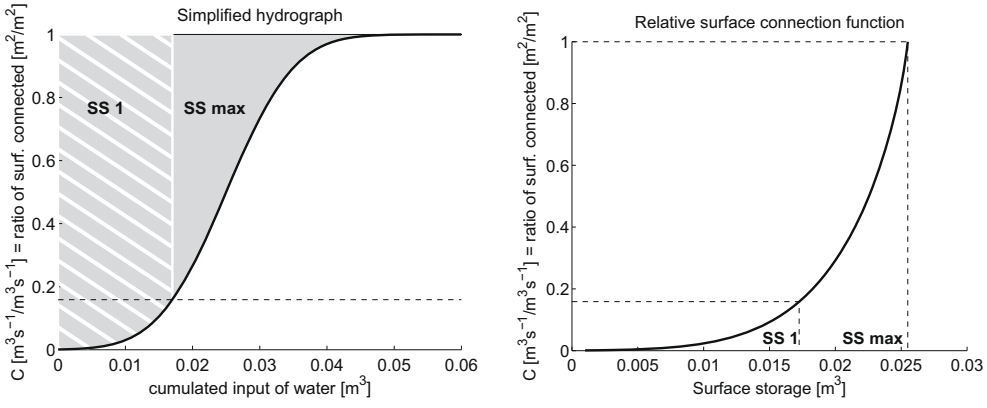

Fig. 2. Simplified hydrograph (left) and the derived relative surface connection function (right).

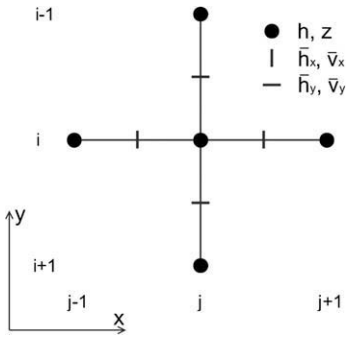

Fig. 3. Two-dimensional fixed grid with the asymmetric velocity computation scheme.

x-direction and y-direction based on Eq. (15). The water level is adjusted in time with the equation of continuity

$$\frac{\partial h}{\partial t} + \frac{\partial \bar{v}_x \bar{h}_x}{\partial x} + \frac{\partial \bar{v}_y \bar{h}_y}{\partial y} = \phi \tag{19}$$

where ϕ is a source term that is equal to the rain rate minus the infiltration rate [m/s]. The latter was set to zero. A classical Courant–Friedrichs–Lewy (**CFL**) condition was used to discretize the time. The model has been validated under laboratory conditions for experimental channels with different hydraulic roughness.

Table 1 shows the comparison between the physical runoff model presented here above and the filling algorithm from the previous section. The physical runoff model can determine the effect of the micro-topography on the live storage, which depends on the runoff velocity (and thus on the rain intensity). It implies the use of a CFL condition that imposes small time steps for our scale of investigation. The requirement of small time steps on top of the iterative computation of the friction factor causes long computation time. In the context of establishing a fast and robust method to determine an indicator of functional connectivity, this long computation time is an issue. As the filling algorithm is more than 1000 times faster than the runoff model, due to the simplification of the runoff routing, it will be used to produce the functional connectivity indicator. The physical runoff model will only serve to predict the expected real hydrographs.

Table 1
Comparison of the physical runoff model and the filling algorithm.

Physical runoff model	Filling algorithm
Input	**Input**
Topography $z(x,y)$	Topography $z(x,y)$
Rain intensity ϕ	
Roughness parameters k_s, C_L	
Kinematic viscosity of the water v	
Output	**Output**
Runoff coefficient $C(t)$	Simplified runoff coefficient C (cumulated inflow)
Water depth field $h(x,y,t)$	Water depth field h (x,y,cumulated inflow)
Velocity fields $\bar{v}_x(x,y,t)$, $\bar{v}_y(x,y,t)$	
Processes	**Processes**
Flow following the slope of water	Flow following the slope of water
Multiple flow, de-centered 4-neighbors scheme	Simple flow, 8-neighbors scheme
Velocity based on Darcy–Weisbach formula	Infinite velocity, water reaches directly the lowest point it can get to
Surface detention and retention (live and dead storage)	Surface retention (dead storage)
Time steps	**Time steps**
Depending on CFL condition ($\overline{\Delta t} \approx 0.001$ s)	Fixed ($\Delta t = 1$ s)
Time of computation	**Time of computation**
Computation time/simulation time = 300	Computation time/simulation time = 0.3

2.4. Case study: synthetic fields

We used the method of Zinn and Harvey [53] to generate the numerical fields of micro-topography. This method allows us to generate fields that have contrasted structural connectivity properties (in our case the way depressions connect or not to each other) while presenting, for the pixels heights, identical probability density functions as well as near-identical isotropic spatial covariance functions. The three types of numerical fields are: (1) a field with connected patterns of depressions, (2) a standard multi-Gaussian field and (3) a field with connected patterns of crests that isolate from each others the depressions. For sake of clarity, we will speak about the River micro-topography for the first field, the Random (with regards to connectivity) micro-topography for the second and the Crater micro-topography for the third one. Let us note that Crater and River surfaces are the exact inverse of one another.

These micro-topographies are fictive and only are useful to verify the relevance (for a later use on real field experiments) of the connectivity indicators when confronted to extreme scenarios. Real micro-topographies will behave intermediately if we assume that, on a same field, some of the depressions will always be well connected while others will remain mostly isolated. And even if the numerical micro-topographies do not fully mimic reality, they are parametrized by realistic values for the sill ($100\ mm^2$) and the range (100 mm) of their semivariograms. Those values were indeed observed on experimental plots [12] and real fields [47]. It is tempting to link the artificial micro-topographies in some way to the temporal evolution of real states of the soil surface. For instance, depressions are mainly isolated from each others just after tillage and form Crater-type topographies [36,8]. Due to the shaping action of the overland flow itself that incises the borders of the crests where water overflows [12], the landscape evolves to create a connected micro-topography [15], such as eroded soil after heavy rain periods, forming River-type topographies [16].

In order to simplify the problem on focusing on one process only, infiltration was left out of the study. In reality, infiltration plays a key role in connectivity disruption. Indeed, runoff water may infiltrate downhill when it reaches places with higher infiltration capacity [5]. Although, we consider at our scale that the overland flow is fed by a uniform and net supply of water of 100 mm/h. A high rain intensity was considered for computation time reasons. This high intensity must long 5–10 min in order to insure that the hydrographs reach their maximum. This type of rain as a return period of 20 years in central Belgium. We also simplified the problem by not taking into account any oriented anthropogenic roughness such as ridges and furrows.

The method of computation and the statistical properties on which it relies is given in Appendix A. The full fields had a size of 2×2 m and were discretized in 0.01×0.01 m cells. In order to test the robustness of the connectivity indicators, we generated 10 fields for each of the 3 contrasted micro-topographies and added a 1% slope effect to all the topographies. Discussion on the effect of the slope is not included in the paper. We assume that slope affects the flow pathways so that connections in the direction of the flow will be favoured as slope increases. Some connections may disappear while new ones may be created. The dead storage decreases with increasing slopes [27,39]. The live storage should decrease when slope increases because, for a same velocity computed by Eq. (15), the depth and the slope can mutuality compensate each other.

An example of one replicate for each of the three micro-topography types is given in Fig. 4.

3. Results

3.1. Effect of the spatial arrangement of micro-topography on the hydrograph

To see if spatial arrangement of the micro-topography (or structural connectivity) had a significant impact on the hydrographs, we simulated runoff, with the physical runoff model based on the diffusive wave equation, for 10 different fields of each micro-topography type (10× Random, 10× Crater and 10× River). Fields, initially water-free, were submitted to a constant rain of 100 mm/h and no infiltration was taken into account. To reduce the computation time, the experiment was conducted on only a quarter of each field (1 m^2). For the different micro-topography types, if distinct hydraulic behaviors already emerge at that scale, this distinction will be enhanced as we consider larger fields due to the decreasing impact of borders effects. Results are shown in Fig. 5.

The River fields are the first to reach the steady state runoff rate that is theoretically equal to the rain intensity (since no infiltration is considered). It is followed by the Random and then by the Crater cases. Although there is some variability among the replicates, there is a clear effect of the micro-topography type. The more the depressions are isolated from each other, the longer it takes for the runoff rate to tend to the rainfall intensity. The main factor is the effect of micro-topography on both the dead surface storage (Crater: 5.3 ± 2.85 mm, Random: 2.91 ± 1.14 mm, River: 1.14 ± 0.56 mm) and live surface storage (Crater: 1.07 ± 0.41 mm, Random: 0.84 ± 0.36 mm, River: 0.51 ± 0.23 mm) that need to be fully filled before reaching steady state. The dead storage is the major factor that distinguishes the different micro-topographies. Therefore, the use of the filling algorithm to produce a functional connectivity indicator appears yet sufficient, despite it does not consider the live storage.

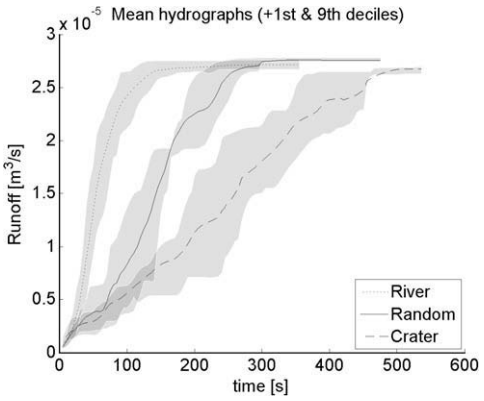

Fig. 5. Impact of the micro-topography type on the hydrograph. The mean runoff values (number of replicates = 10) are given for each micro-topography type as well as the envelop limited by the 1st and 9th deciles.

For all the scenarios, the random roughness of the fields is equivalent ($\sigma_z = 0.01$ m), and thus is not a good proxy to determine the surface storage, in contrast to the results of Kamphorst et al. [27]. This demonstrates the interest of the small scale connectivity to correctly model the hydrographs at the beginning of a

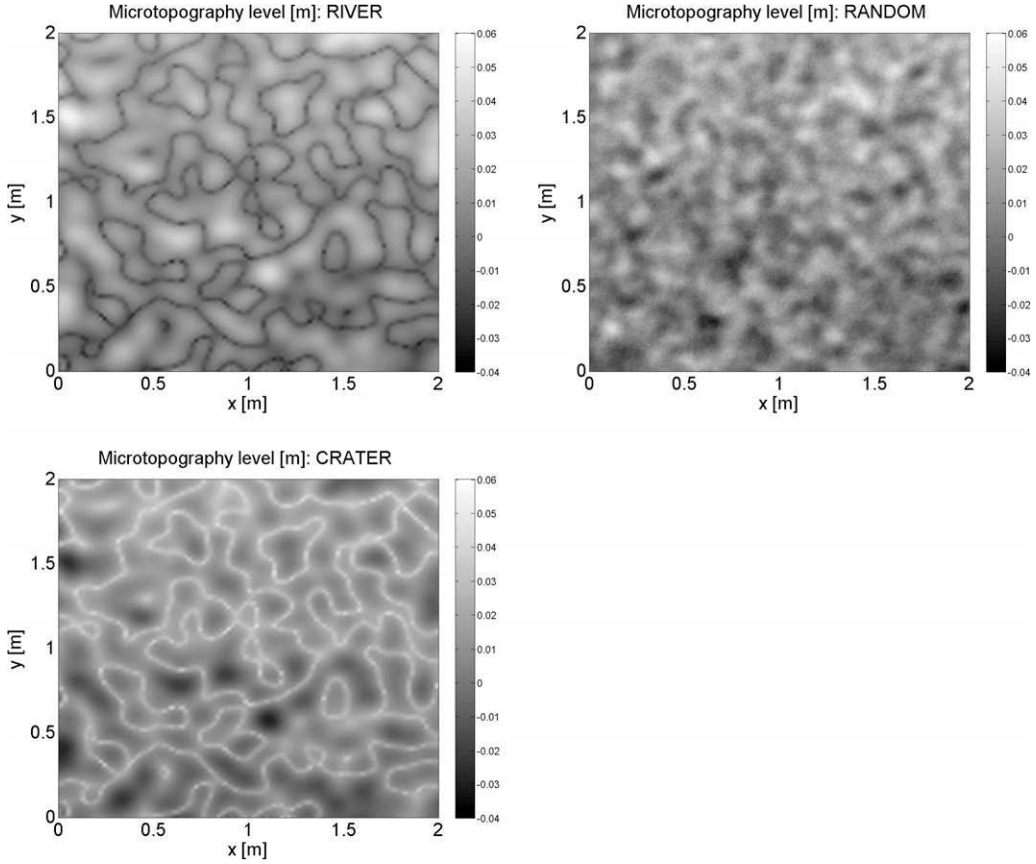

Fig. 4. River, Random and Crater micro-topographies (the color of the pixels corresponds to the surface height). The mean altitude decreases from the top to the bottom of the images with a 1% slope (grid cells: 1 cm × 1 cm).

rainfall. Therefore we need to identify robust indicators of connectivity computed from the topography. This is done in the following sections.

3.2. Robustness of the structural connectivity indicators

The robustness of the structural connectivity indicators was tested by computing these indicators for 10 realizations of each of the three types of micro-topography and assessing the variability within and in-between the three types of topography. We consider as relevant the connectivity indicators that are able to discriminate the three micro-topography types, whatever the fields.

The computations of the semivariograms, the bivariate entropy and the *n*-point rectilinear connectivity do not require a full knowledge of the micro-topography. Since they are statistical properties, semivariogram and entropy may be established only on a reduced sample of the micro-topography, as long as the resolution is sufficiently smaller than the correlation length and the domain investigated at least twice as large as this length. The *n*-point rectilinear connectivity only requires knowledge of a 1D topographical profile in the mean slope direction. For practical assessment at the field, this can easily be achieved with a classical rugosimeter [18]. Therefore, these three indicators present some practical advantages. However, as we see in Fig. 6, the three methods do not sufficiently discriminate between the three micro-topography types. These indicators are therefore not considered as relevant structural connectivity indicators.

The other structural connectivity indicators (connectivity function, Euler number and percolation probability) require the full knowledge of the micro-topography (which in practice requires more sophisticated tools such as laser technique), because their computation takes into account all the possible connections in 2D. Fig. 7 presents these structural connectivity indicators. For all three indicators, the river scenarios tend to increase more rapidly as the threshold level z is increased, followed by the intermediate cases (random) and finally by the Crater micro-topographies. The visual inspection of these three last indicators shows their discriminative capacity.

3.3. Robustness of the functional connectivity indicator

Fig. 8 (left) shows the results for the simplified hydrographs. There is a clear distinction between micro-topography types. For the Crater micro-topography, a larger input of water is necessary before outflow equals inflow. Since no infiltration was taken into account, the water added to the system that did not produce runoff was stored in local depressions and represents the actual surface storage. After a sufficient cumulative input of water, this area does not increase anymore. At that stage, all the potential surface storage has been fully filled and corresponds to the maximal dead storage. It can be regarded as the volume to full breakthrough.

Based on the scaled hydrographs, we can derive the relative surface connection function. This is shown in Fig. 8 (right). It clearly shows that maximal surface storage is higher for the Crater micro-topography than for the river micro-topography, in an approximate 5 to 1 ratio. Secondly, we clearly see that surface storage does not have to be entirely filled before significant runoff is produced. As already shown by Moore and Larson [35], storage and runoff amounts increase continuously as water accumulates in micro-depressions, but the percentage of area contributing to runoff increases by steps. Although a widely-used simplification made in hydrological modelling is that no runoff can occur before the total surface storage is fully filled [42,43], and so there is no contributing area before the fully filling of that surface storage.

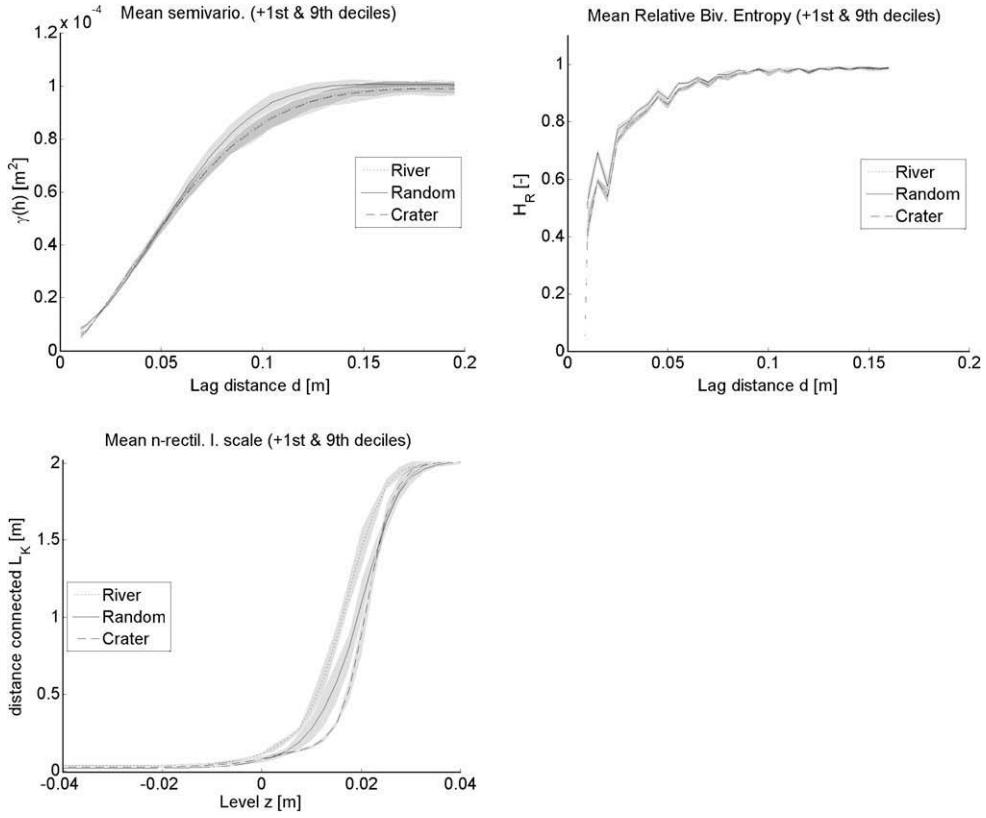

Fig. 6. Semivariograms (top left), relative bivariate entropy (top right) and *n*-point rectilinear connectivity integral scale (bottom left) calculated for 10 realizations of each of the Crater, Random and River-type micro-topographies. The mean values are given for each micro-topography type as well as the envelop limited by the 1st and 9th deciles.

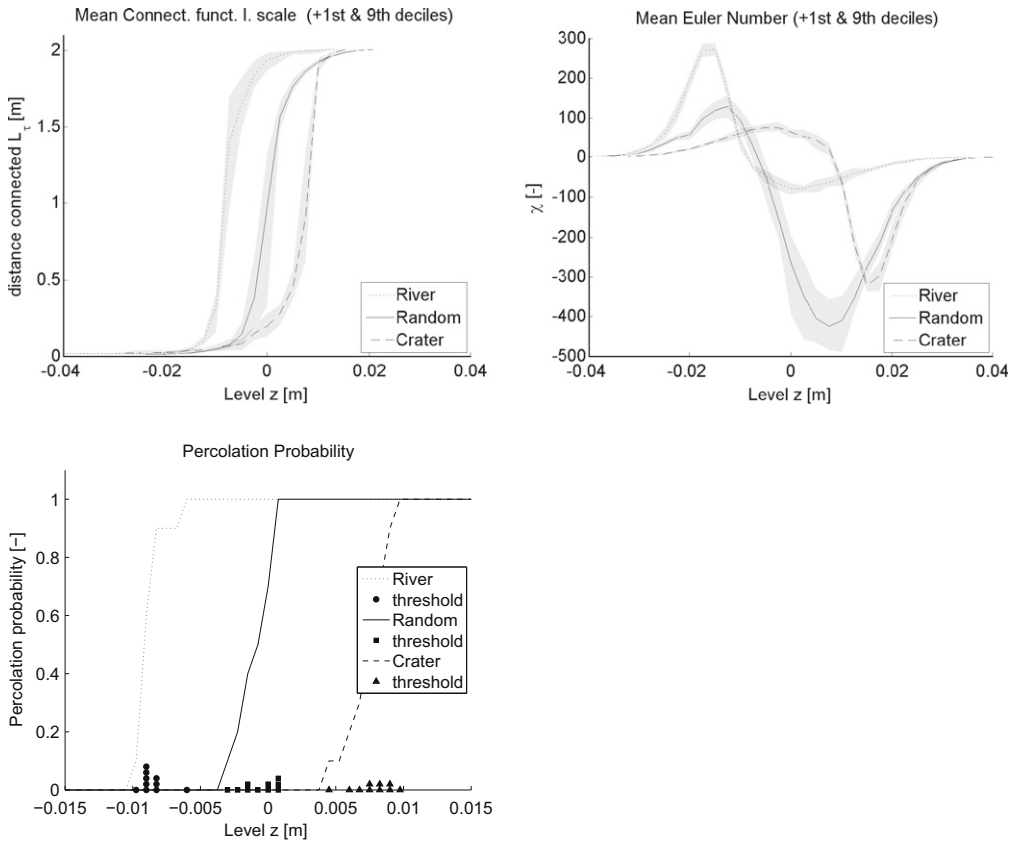

Fig. 7. Connectivity function integral scale, Euler number and Percolation thresholds with the derived Percolation probability curve, calculated for 10 realizations of each of the three micro-topographical types: River, Random and Crater. The mean values are given for each micro-topography type as well as the envelop limited by the 1st and 9th deciles.

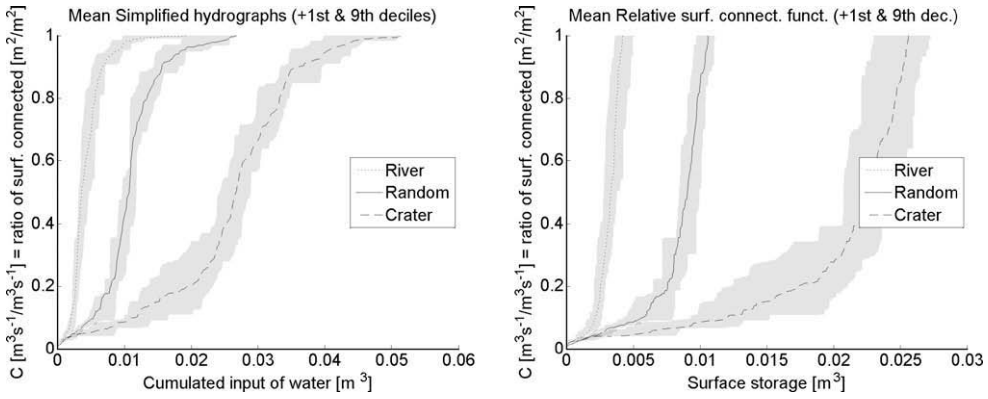

Fig. 8. Simplified hydrographs (left) and derived relative surface connection functions (right). The mean values (number of replicates = 10) are given for each micro-topography type as well as the envelop limited by the 1st and 9th deciles.

4. Discussion

Table 2 summarizes the indicators for structural and functional connectivity investigated in this study.

4.1. Robustness of the structural connectivity indicators: success and failures

Semivariograms were not able to distinguish the different micro-topography types because the scenarios were built with a method that was specifically conceived to blur the structure to the semivariogram. All fields have a similar distribution thanks to the back-transformation given in Eq. (27) of Appendix A. Despite the fact that this transformation is non-linear, Zinn and Harvey [53] showed that the covariance between points separated by a lag distance was little affected if a scale factor was considered to preserve the integral scale of the correlation coefficient. The semivariograms are rectilinear in that they do not take into account the curvilinearity of the structures [30] and so they are not appropriate to capture connectivity. This confirms the results of Western et al. [51], Grayson et al. [17].

Relative bivariate entropy depends directly on the bivariate PDF. For two random variables $\zeta \sim N(\mu, \sigma)$ and $\zeta' \sim N(\mu', \sigma')$ both normally distributed, their bivariate PDF is expressed by:

Table 2
Summary of the structural and functional connectivity indicators investigated in this study.

Connectivity indicator	Connectivity type	Information requirement	Binarization procedure	Is the indicator discriminant?
(1) Semivariogram	Structural	Sampling points	None	No
(2) Relative bivariate entropy	Structural	Sampling points	None	No
(3) n-Point rectilinear connectivity	Structural	Transect information	By watershed rules	No
(4) Connectivity function integral scale	Structural	Full knowledge	By watershed rules	Yes
(5) Euler number	Structural	Full knowledge	Threshold-based	Yes
(6) Percolation thresholds	Structural	Full knowledge	By watershed rules	Yes
(7) Relative surface connection function	Functional	Full knowledge	None	Yes

$$f_h(\zeta,\zeta') = \frac{1}{2\pi\sigma\sigma'\sqrt{1-\rho^2}} \exp\left[-\frac{1}{2(1-\rho^2)}\left(\left(\frac{\zeta-\mu}{\sigma}\right)^2 - \frac{2\rho(\zeta-\mu)(\zeta'-\mu')}{\sigma\sigma'} + \left(\frac{\zeta'-\mu'}{\sigma'}\right)^2\right)\right] \quad (20)$$

where μ and μ' are the means, σ and σ' are the standard deviations and ρ is the correlation coefficient defined by:

$$\rho_{\zeta\zeta'} = \frac{Cov[\zeta,\zeta']}{\sqrt{Var[\zeta]Var[\zeta']}} \quad (21)$$

By keeping $\mu, \mu', \sigma, \sigma'$ and ρ constant between the different scenarios, we leave the bivariate PDF unchanged. If ζ represents the variable values at the locations $\mathbf{x}$ and ζ' at the location $\mathbf{x}+\mathbf{d}$, because of the stationarity of order 1 and 2 of the Gaussian fields, we know that $\mu = \mu',\ \sigma = \sigma'$. Moreover, thanks to the renormalization procedure (Eq. (27)), μ and σ keep the same values whatever the fields. $\rho_{\zeta\zeta'}$ can be directly determined from the semivariograms, since by stationarity of order 2:

$$\gamma(\mathbf{d}) = \sigma^2 - Cov[\mathbf{x}, \mathbf{x}+\mathbf{d}] \quad (22)$$

If the semivariograms $\gamma(\mathbf{d})$ are similar, for a fixed lag distance $\mathbf{d}$, the covariance and thus the correlation coefficient will also be similar. All factors of the bivariate PDF are kept constant whatever the scenarios and leave the entropy unchanged. Therefore, entropy, like the semivariograms, can not distinguish between the three micro-topography types.

N-direct connectivity does not take into account the curvilinearity of the structures [30]. Any obstacle in the way of the flow would be considered as a definitive stop, although in reality water could flow around that obstacle. Some linear connected features in the axis of the mean slope are still captured. This explains why the indicator could slightly discriminate between the three topographic types (curves are juxtaposed next to each other in function of the type). However, as there are some overlap between curves of different topographical types, this indicator was considered insufficiently robust.

The connectivity function integral scale represents an equivalent mean distance from the outlet up to which the surface is connected. Its value is between 0 up to the maximal distance of the field (in our case 2 m). This function, which is the equivalent of the n-connectivity function but takes into account the possibility of the runoff to flow in two dimensions around the obstacles, improves a lot the discrimination between the three micro-topography types. The main assumption, due to the choice of binarization process, is that the water in all the depressions is at the same absolute level, which is not valid in practice since depressions have different storage volumes and drainage areas. Moreover, the outlet is considered as a depression that fills in. The result is an over-estimation of the mean water level in the system to ensure the full connection of the surface. Nevertheless this gives us already a rough estimation of the relation between the surface storage and the surface connectivity if we transform the level into a surface storage

$$SS = S\int_{-\infty}^{z} P(Z \leqslant z)\partial z \quad (23)$$

where SS is the surface storage [m^3] and S is the surface of the field [m^2].

Take note that since all three micro-topography types have the same distribution, $P\ (Z \leqslant z)$ will be equivalent for them whatever z. So the relation between the surface storage and the z-level will be the same for the different cases.

Percolation probability is a cumulative density function (CDF) and requires all the 10 scenarios to represent it. All the threshold values (presented as geometric symbols in Fig. 7 (bottom left) are well grouped as a function of the micro-topography types. Hence, this indicator is capable of discriminating the topography type. It is a measure of the continuity between the upstream and downstream ends of the topographical fields, yet it provides no information on how the continuity of the water field evolves as the water level is raised. This type of indicator is therefore of no use to characterize the within-field connectivity, but it may be of use to characterize the connectivity between adjacent fields. Indeed, water produced upstream on a slope will only join the downstream drainage network if all the patches that it needs to cross are all at least at the percolation threshold. Hence those values could be useful for subsequent upscaling of the runoff process, but this falls beyond the scope of this paper. The percolation thresholds reported here are not in adequacy with standard percolation theory, since in our case pixels are in the field of interest according to watershed rules and not according to a certain level of probability of occurrence equally distributed over the entire field, as in percolation theory.

Euler number χ presents some discriminative properties. The curves for all the fields present a similar shape that is due to a same behavior: as the threshold level z is increased, more and more pixels are in the field of interest due to the binarization procedure. Those pixels are, in the beginning, often isolated from each others (N increases) and we find few connections (G is comparatively low). This increases the Euler number ($\chi = N - G$). After a certain threshold level (z_a), the previously isolated patches tend to connect to each other progressively. The Euler number begins to decrease as the number of multiple connections (G) increases between the patches. Rising again the threshold level z, particular patches begin to merge (N decreases), which erases their previous multiple interconnections (G decreases faster than N). This increases again the Euler number. We see that z_a is lower for the River micro-topography for which depressions quickly connect to each other as opposed to the Crater micro-topography. We also see that z_a is not so different between River and Random micro-topographies. But the χ-value reached by the former one is lower than for the latter. This means that the Random cases are more chaotic as the number of interconnections explodes (but thus are less strong) whereas the River cases keep relatively few but stable connections. As we see,

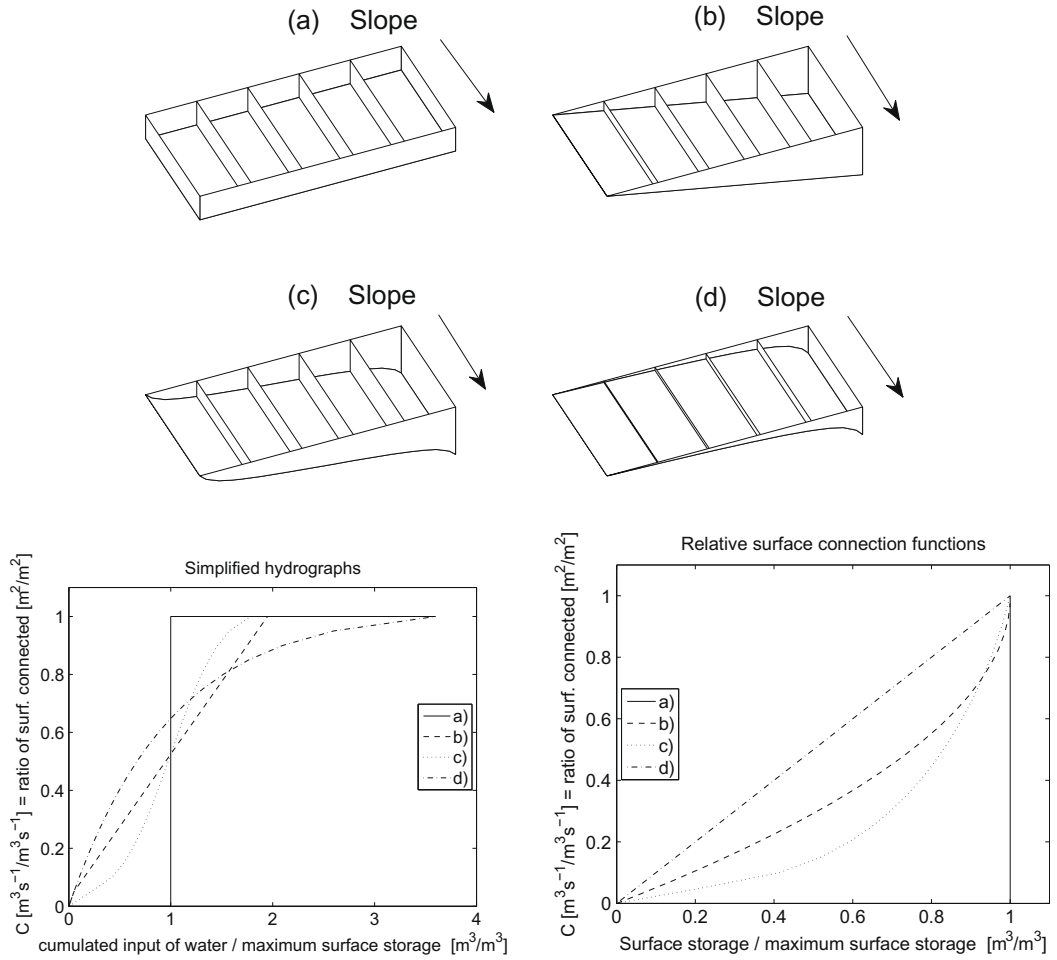

Fig. 9. Conceptual multiple boxes topographies, their simplified hydrographs and their derived relative surface connection functions. The local storage depths are distributed according to: (a) a single value, (b) a uniform distribution, (c) a Gaussian distribution, and (d) a particular distribution so that the relative surface connection function is linear.

the change in Euler number with increasing water level contains information on the dynamics of pond formation.

4.2. Robustness of the functional connectivity indicator: Success and development

Simplified hydrographs and especially the derived **relative surface connection functions** were clearly able to discriminate the three micro-topography types. River structures improve the evacuation of the water and reduce the surface storage, while Crater structures favour water retention on the field. Simplified hydrographs are shifted to the right as maximum surface storage increases. A theoretical framework is proposed (see Fig. 9) to correlate the local surface storage distribution to the simplified hydrographs and to the relative surface connection. The four conceptual surfaces have the same maximum surface storage but the intrinsic repartition of the surface storage differs. The first case (a) is an on/off type of surface. All the local depressions of the field have equivalent storage capacity (i.e., the ratio between particular depressions volumes and their respective contributing areas are constant). Thus the actual surface storage will have to reach the maximum surface storage value before runoff occurs. As outlined before, it is a widely-used simplification made in hydrological modelling. The second case (b) is a surface whose local storage values are distributed uniformly. A droplet of rain therefore has the same probability of filling a small depression, than a medium or a large one. It will produce a linear simplified hydrograph. For the third case (c), local storage values follow a Gaussian distribution. The simplified hydrograph has a sigmoid form. The last case (d) accounts for a surface whose relative surface connection function evolves linearly with the filling of the surface storage. It corresponds to the case $k = \frac{1}{SS_{max}}$ for the Linsley et al. [32] equation of the surface storage filling:

$$SS = SS_{max}(1 - \exp(-kQ_{inC})) \tag{24}$$

where SS is the surface storage value [m^3], SS_{max} is the maximal surface storage [m^3], k is a constant [m^{-3}] and Q_{inC} is the cumulated input of effective rain [m^3].

We established the mathematical expressions for the simplified hydrographs and the relative surface connection functions (Tables 3 and 4). Those simple models are parametrized by few parameters (1 or 2): the maximal surface storage only (a, b, d) or the maximal surface storage and a shape factor (c). A combination of the (a) case with the three others (b, c, d) is easily implemented by subtracting an initial value to the cumulated rain and to the actual surface storage (i.e., LISEM v 1.63 and earlier is a combination of (a) and (d)[1]). In terms of functional connectivity, the quicker the curve of surface connection rises, the more reactive the surface is to rain input. The (d) case reacts like that. An extreme case would be the existence of one deep depression that would account for most of the total

[1] http://www.itc.nl/lisem/index.html.

Table 3
Mathematical expressions of the simplified hydrographs presented in Fig. 9 for the different conceptual multiple boxes topographies.

Surface storage distribution	Simplified hydrograph $C = \frac{Q_{out}}{Q_{in}} = f(Q_{inC})$
(a) Single value	$f(Q_{inC}; SS_{max}) = \begin{cases} 0 & \text{if } Q_{inC} < SS_{max} \\ 1 & \text{else} \end{cases}$
(b) Uniform	$f(Q_{inC}; SS_{max}) = \begin{cases} \frac{Q_{inC}}{2SS_{max}} & \text{if} Q_{inC} < 2SS_{max} \\ 1 & \text{else} \end{cases}$
(c) Gaussian	$f(Q_{inC}; \mu \approx SS_{max}, \sigma) = \frac{1}{2}\left(1 + \text{erf}\left(\frac{Q_{inC}-\mu}{\sigma\sqrt{2}}\right)\right)$
(d) Specific so that $C \propto SS$	$f(Q_{inC}; SS_{max}) = -\exp\left(-\frac{Q_{inC}}{SS_{max}}\right) + 1$

With Q_{out} the runoff [m^3/s], Q_{in} the input of rain [m^3/s], Q_{inC} the cumulated input of rain [m^3], SS the actual surface storage [m^3], SS_{max} the maximal surface storage [m^3], μ a factor approximatively equal to SS_{max} [m^3] and σ a factor of dispersion [m^3].

Table 4
Mathematical expressions of the relative surface connection functions presented in Fig. 9 for the different conceptual multiple boxes topographies.

Surface storage distribution	Relative surface connection function $C = \frac{S_{connected}}{S_{tot}} = g(SS)$
(a) Single value	$g(SS; SS_{max}) = \begin{cases} 0 & \text{if } SS < SS_{max} \\ 1 & \text{if } SS = SS_{max} \end{cases}$
(b) Uniform	$g(SS; SS_{max}) = 1 - \sqrt{1 - \frac{SS}{SS_{max}}}$
(c) Gaussian	$g(SS; \mu \approx SS_{max}, \sigma) = \frac{1}{2}\left(1 + \text{erf}\left(\frac{Q_{inC}(SS)-\mu}{\sigma\sqrt{2}}\right)\right)$, where $SS(Q_{inC}) = h\left(Q_{inC}; \alpha = \frac{1}{\sigma\sqrt{2}}, \beta = \frac{-\mu}{\sigma\sqrt{2}} \approx \frac{-SS_{max}}{\sigma\sqrt{2}}\right)$ $= \frac{1}{2}\left(Q_{inC} + \mu - \frac{\beta \text{erf}(\delta)}{\alpha} - Q_{inC}\text{erf}(\delta) - \frac{\exp(-(\delta)^2)}{\alpha\sqrt{\pi}}\right)$ with $\delta = \beta + \alpha Q_{inC}$
(d) Specific so that $C \propto SS$	$g(SS; SS_{max}) = \frac{SS}{SS_{max}}$

$S_{connected}$ the surface connected to the downstream boundary [m^2], S_{tot} the total surface [m^2], SS the actual surface storage [m^3], SS_{max} the maximal surface storage [m^3], μ a factor approximatively equal to SS_{max} [m^3], σ a factor of dispersion [m^3] and Q_{inC} the cumulated input of rain [m^3].

surface storage, but that would only be fed by a small part of the total surface. In that case, even if the actual surface storage would be low, most of the surface would be well connected and would participate to the export of runoff. Connectivity increases thus passing from the (a) to (c), (b) and (d) conceptual fields (except for relative storage close to 1).

We can now chose either to work with the true simplified hydrographs and derived relative surface connection functions or either to parametrize them with one (or a combination) of the simplified models (a, b, c, d). This last option may be useful for later upscaling procedure or for regular implementation in actual hydrological models. Our observations were best fitted with the Gaussian model (c). Results are shown in Fig. 10. The factor μ_{BC} (from Tables 3 and 4) is almost equivalent to the maximum surface storage and we have imposed this value. The factor σ is a formal factor that accounts for the spread of the simplified hydrographs. The lower its value the sharper the hydrograph. When σ tends to zero, then case (c) tends to case (a) with a step hydrograph. On the contrary, the larger the sigma, the higher the potential connectivity is. We compare the dispersion of the fitted parameters in Fig. 11. The μ and σ factors are distinct between the micro-topography types, but the coefficient of variations are alike for all the micro-topographies meaning that the repartition of local surface stores are comparatively similar. This means that if the pixels height values of a River-type micro-topographical field were all multiplied by a unique scaling factor, the new field may produce a similar hydrograph as the one for a Crater-type field. This may come from the method used to build the different micro-topographical fields.

4.3. The scale problem

The spatial resolution of the digital elevation model for the micro-topography is determinant for the computation of its connectivity properties. The key elements are the small channels that link the depressions together. Those can be missed if the spatial resolution is too low. As stated by Western et al. [51], the apparent presence of near connectedness is scale dependent. The evaluation of the retention capacity of the depressions is also dependent on the resolution. Real concavities or convexities between the points of measurement can be ignored by the interpolating methods, resulting in an underestimating or an overestimating of the depression volume respectively. In summary, the resolution plays a role on the connections identification and on the storage evaluation.

Carvajal et al. [8] and Martin et al. [33] both observed a decrease of maximal surface storage when pixels size increased (from a mm to a 2 cm scale resolution for the first study, and from the centimeter to a half meter scale for the second). In contrary, Abedini et al. [1] found an increase followed occasionally by a decrease of the ponds volume when pixel size increased from a 5 mm to 3 cm scale resolution. Kamphorst et al. [27] did not observe significant change in maximum surface storage when passing from a mm to a 2 cm scale resolution. The effect of the resolution is thus not obvious and the strategy is to adapt the resolution in function of the correlation lengths of the field and the size of the connectors.

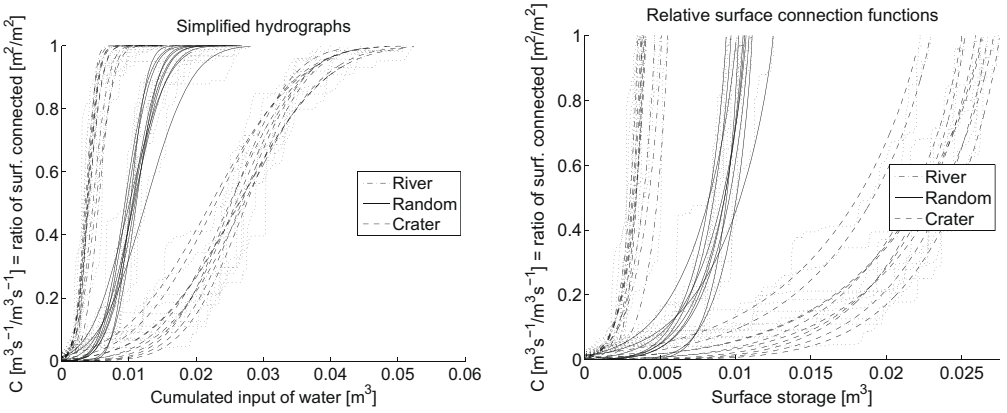

Fig. 10. Fitted simplified hydrographs (left) and derived fitted relative surface connection functions (right). Gaussian model (c) was used for the fitting. The gray dotted lines are the fitted curves.

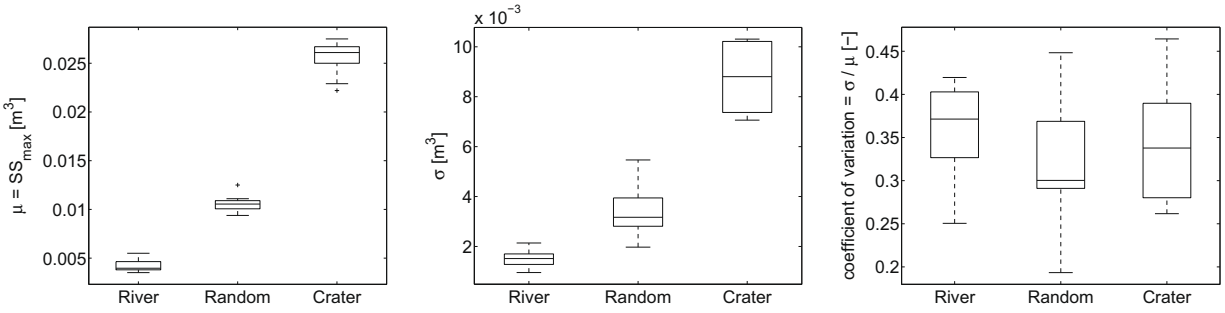

Fig. 11. Box plots of the fitted μ or maximum surface storage (left), the fitted σ (center) and the coefficients of variation (right) for the three contrasted micro-topographies. Gaussian model (c) was used for the fitting.

5. Conclusion

- Independently of the random roughness value, the spatial organization of the micro-topography affected the live storage (surface detention) of our contrasted scenarios in a ratio of 1 to 2, and the dead storage (surface retention) in a ratio of 1 to more than 4, under a constant and uniform net rain supply to the overland flow. Surface connectivity of the micro-topography plays thus an important role on the runoff triggering and on the shape of the hydrograph, and needs to be quantitatively evaluated.
- The semivariogram, the bivariate entropy and the n-point rectilinear connectivity are structural connectivity indicators that were not able to discriminate clearly the contrasted micro-topographies. Therefore, we think that those methods must not be used to study the structural connectivity of natural micro-topographies unless they are improved to integrate spatial patterns.
- The connectivity function integral scale, the percolation probability and the Euler number are structural connectivity indicators that had a discriminative capacity. Whereas the connectivity function integral scale and Euler number provide information regarding the development of connectivity within topographical fields, the percolation threshold appears more suitable to characterize connectivity between adjacent fields. In any case, despite their discriminating power, relating the latter three structural connectivity indicators to the hydrological response of a topographical surface will prove to be a challenging task.
- We proposed a functional connectivity indicator, namely the relative surface connection function, that is the ratio of surface connected in function of the actual surface storage. It was computed using a fast and simple filling algorithm that produces simplified hydrographs based only on the dead storage dynamic. The simulation had shown indeed that the dead storage was the major factor of discrepancies between our contrasted scenarios. This indicator was discriminant and could be used to conceptualize the process of depression filling. Once computed for a small surface, this function could become a descriptive function of the subgrid dynamics to be integrated in hillslope or watershed models for which the surface considered for the computation of the connectivity indicator corresponds then to a single grid cell. We recommend this indicators as it requires the same information than the discriminant structural indicators, it is almost as fast to compute, but it contains information more directly linkable to runoff dynamic.
- At this stage, the proposed functional connectivity indicator does not take into account the upper boundary conditions, i.e., the effect of rainfall intensity, nor the live storage dynamics. This effect should be integrated in an effective way to correct the present functional connectivity indicator. Moreover, the effect of the infiltration, the effect of the slope as well as the effect of the spatial resolution of the elevation data are to be investigated. Finally, the successful indicators are now to be applied on real field data. All this is part of our ongoing research.

Appendix A. Numerical fields generation

The method proposed by Zinn and Harvey [53] is based on the following probabilistic property. Given a continuous random variable Y characterized by any kind of cumulative density function $F_y(y)$ ($Y \sim F_y$) and another random variable X uniformly distributed between 0 and 1 ($X \sim Un(0,1)$), it can be shown that $Y = F_y^{-1}(X)$ [4]. This method is used to generate series that follow any kind of distribution $F_y(y)$ starting with series of uniformly distributed variables. Conversely, given a continuous random variable Z characterized by any kind of cumulative density function $F_z(z)$, the random variable X uniformly distributed between 0 and 1 can be generated by applying $X = F_z(Z)$. Combining the two approaches, we can then generate Y based on Z by transforming successively Z into X and X into Y. Thus $Y = F_y^{-1}(F_z(Z))$.

To generate their fields, Zinn and Harvey [53] propose a four-steps procedure that starts with the generation of a multi-Gaussian field Y, using a conditional simulation method. Since the link between their method and the concept we explained in the previous paragraph is not described in their article, we provide some more details.

$$Y \sim N(\mu, \sigma^2) \tag{25a}$$

$$\Rightarrow F_Y(y) = \frac{1}{2}\left(1 + \mathrm{erf}\left(\frac{y-\mu}{\sigma\sqrt{2}}\right)\right) \tag{25b}$$

$$\Rightarrow F_Y^{-1}(y) = \mathrm{erf}^{-1}(2y-1)\sigma\sqrt{2} + \mu \tag{25c}$$

Extreme values in the field tend to cluster in isolated blobs while values close to the mean tend to form channels that span the entire field. The second step is to generate a new field Z by taking the absolute value of the centered multi-Gaussian field Y. The lowest values become the highest and values originally close to the mean (i.e. the well connected) become the lowest.

$$Z = |Y - \mu| \tag{26a}$$

$$\Rightarrow F_Z(z) = P(Z \leqslant z) \tag{26b}$$

$$\Rightarrow F_Z(z) = P(|Y-\mu| \leqslant z) = P(-z \leqslant Y - \mu \leqslant z) \tag{26c}$$

$$\Rightarrow F_Z(z) = P(Y - \mu \leqslant z) - P(Y - \mu \leqslant -z) \tag{26d}$$

$$\Rightarrow F_Z(z) = P(Y - \mu \leqslant z) - (1 - P(Y - \mu \leqslant z)) \tag{26e}$$

$$\Rightarrow F_Z(z) = 2P(Y - \mu \leqslant z) - 1 = 2F_{Y-\mu}(z) - 1 \tag{26f}$$

$$\Rightarrow F_Z(z) = 2\frac{1}{2}\left(1 + \mathrm{erf}\left(\frac{z-0}{\sigma\sqrt{2}}\right)\right) - 1 = \mathrm{erf}\left(\frac{z}{\sigma\sqrt{2}}\right) \tag{26g}$$

In a third step, the histogram of the values is then converted back to a univariate Gaussian distribution by mapping the Cumulative Density Function (CDF) value at each point to a standard normal CDF. This transformation is the application of the probabilistic property explained above.

$$Y' = F_Y^{-1}(F_Z(Z)) = \mathrm{erf}^{-1}\left(2\mathrm{erf}\left(\frac{|Y-\mu|}{\sigma\sqrt{2}}\right) - 1\right)\sigma\sqrt{2} + \mu \quad (27)$$

Y' are the transformed values and Y are the original values. This method will produce a field Y' where the lowest values will be connected. This is used to generate the River micro-topography. In order to generate the Crater micro-topography, with the highest values connected, the values of the previous field Y' are reflected around the mean to create the new field Y''. This operation preserves the mean and the standard deviation

$$Y'' = 2E[Y'] - Y' \quad (28)$$

Zinn and Harvey [53] demonstrated that spatial correlations are almost kept if a scale factor is taken into account.

References

[1] Abedini MJ, Dickinson WT, Rudra RP. On depressional storages: the effect of dem spatial resolution. J Hydrol 2006;318:138–50.
[2] Allard D, HERESIM-Group. Geostatistic Troia'92, vol. 1. Norwell, MA: Kluwer Acad., 1993. p. 467–78 [Ch. On the connectivity of two random set models: the truncated Gaussian and the Boolean].
[3] Bellin N, van Wesemael B, Meerkerk A, Vanacker V, Barbera GG. Abandonment of soil and water conservation structures in mediterranean ecosystems a case study from south east Spain. Catena 2009;76:114–21.
[4] Bogaert P. Probabilités pour Scientifiques et Ingénieurs. Ch. Nombres aléatoires. De Boeck Univ., 2005. p. 228.
[5] Bracken LJ, Croke J. The concept of hydrological connectivity and its contribution to understanding runoff-dominated geomorphic systems. Hydrol Process 2007;21(13):1749–63.
[6] Cammeraat LH. A review of two strongly contrasting geomorphological systems within the context of scale. Earth Surf Process Landforms 2002;27(11):1201–22.
[7] Cappelaere B, Touma J, Peugeot C. A recursive algorithm for connectivity analysis in a grid; application to 2d hydrodynamic modelling in heterogeneous soils. Comput Geosci 2000;26(2):121–35.
[8] Carvajal F, Aguilar MA, Aguera F, Aguilar FJ, Giraldez JV. Maximum depression storage and surface drainage network in uneven agricultural landforms. Biosyst Eng 2006;95:281–93.
[9] Cerdan O, Le Bissonnais Y, Govers G, Lecomte V, van Oost K, Couturier A, et al. Scale effect on runoff from experimental plots to catchments in agricultural areas in normandy. J Hydrol 2004;299(1–2):4–14.
[10] Chetkiewicz CLB, Clair CCS, Boyce MS. Corridors for conservation: integrating pattern and process. Annu Rev Ecol Evol Systemat 2006;37:317–42.
[11] Chow VT, Maidment DR, Mays LW. Applied hydrology. McGraw-Hill Publishing Co.; 1988.
[12] Darboux F, Davy P, Gascuel-Odoux C, Huang C. Evolution of soil surface roughness and flowpath connectivity in overland flow experiments. Catena 2002;46(2–3):125–39.
[13] Deutsch CV. Fortran programs for calculating connectivity of three-dimensional numerical models and for ranking multiple realizations. Comput Geosci 1998;24(1):69–76.
[14] Esteves M, Faucher X, Galle S, Vauclin M. Overland flow and infiltration modelling for small plots during unsteady rain: numerical results versus observed values. J Hydrol 2000;228(3–4):265–82.
[15] Favis-Mortlock D. A self-organizing dynamic systems approach to the simulation of rill initiation and development on hillslopes. Comput Geosci 1998;24(4):353–72.
[16] Gomez JA, Nearing MA. Runoff and sediment losses from rough and smooth soil surfaces in a laboratory experiment. Catena 2005;59:253–66.
[17] Grayson RB, Bloschl G, Western AW, McMahon TA. Advances in the use of observed spatial patterns of catchment hydrological response. Adv Water Resour 2002;25(8–12):1313–34.
[18] Guillobez S, Arnaud M. Regionalized soil roughness indices. Soil Tillage Res 1998;45(3–4):419–32.
[19] Guntner A, Seibert J, Uhlenbrook S. Modeling spatial patterns of saturated areas: an evaluation of different terrain indices. Water Resour Res 2004;40(5):W05114.
[20] Gustafson EJ. Quantifying landscape spatial pattern: What is the state of the art? Ecosystems 1998;1(2):143–56.
[21] Heathwaite AL, Quinn PF, Hewett CJM. Modelling and managing critical source areas of diffuse pollution from agricultural land using flow connectivity simulation. J Hydrol 2005;304(1–4):446–61.
[22] Henderson FM. Open channel flow (Macmillan series in civil engineering). Prentice Hall; 1966.
[23] Hirsch LM, Schuette JF. Graph theory applications to continuity and ranking in geologic models. Comput Geosci 1999;25(2):127–39.
[24] Hunt AG. Continuum percolation theory for saturation dependence of air permeability. Vadose Zone J 2005;4(1):134–8.
[25] Imeson AC, Prinsen HAM. Vegetation patterns as biological indicators for identifying runoff and sediment source and sink areas for semi-arid landscapes in Spain. Agric Ecosyst Environ 2004;104(2):333–42.
[26] Journel AG, Deutsch CV. Entropy and spatial disorder. Math Geol 1993;25(3):329–55.
[27] Kamphorst EC, Jetten V, Guerif J, Pitkanen J, Iversen BV, Douglas JT, et al. Predicting depressional storage from soil surface roughness. Soil Sci Soc Am J 2000;64(5):1749–58.
[28] Knudby C, Carrera J. On the relationship between indicators of geostatistical, flow and transport connectivity. Adv Water Resour 2005;28(4):405–21.
[29] Knudby C, Carrera J. On the use of apparent hydraulic diffusivity as an indicator of connectivity. J Hydrol 2006;329(3–4):377–89.
[30] Krishnan S, Journel AG. Spatial connectivity: from variograms to multiple-point measures. Math Geol 2003;35(8):915–25.
[31] Lehmann P, Hinz C, McGrath G, Tromp-van Meerveld HJ, McDonnell JJ. Rainfall threshold for hillslope outflow: an emergent property of flow pathway connectivity. Hydrol Earth Syst Sci 2007;11(2):1047–63.
[32] Linsley RK, Kohler MA, L PJ. Applied hydrology. New York: McGraw-Hill; 1949.
[33] Martin Y, Valeo C, Tait M. Centimetre-scale digital representations of terrain and impacts on depression storage and runoff. Catena 2008;75:223–33.
[34] Mathias SA, Butler AP, McIntyre N, Wheater HS. The significance of flow in the matrix of the chalk unsaturated zone. J Hydrol 2005;310:62–77.
[35] Moore ID, Larson CL. Estimating micro-relief surface storage from point data. Trans ASAE 1979;22(5):1073–7.
[36] Moreno RG, Alvarez MCD, Alonso AT, Barrington S, Requejo AS. Tillage and soil type effects on soil surface roughness at semiarid climatic conditions. Soil Tillage Res 2008;98:35–44.
[37] Neuweiler I, Cirpka OA. Homogenization of richards equation in permeability fields with different connectivities. Water Resour Res 2005;41(2):W02009.
[38] Pardo-Iguzquiza E, Dowd PA. Connec3d: a computer program for connectivity analysis of 3d random set models. Comput Geosci 2003;29(6):775–85.
[39] Reaney SM, Bracken LJ, Kirkby MJ. Use of the connectivity of runoff model (crum) to investigate the influence of storm characteristics on runoff generation and connectivity in semi-arid areas. Hydrol Process 2007;21(7):894–906.
[40] Samouelian A, Vogel HJ, Ippisch O. Upscaling hydraulic conductivity based on the topology of the sub-scale structure. Adv Water Resour 2007;30(5):1179–89.
[41] Scheibe T. Characterization of the spatial structuring of natural porous media and its impacts on subsurface flow and transport. PhD thesis, Stanford University, 1993.
[42] Singh VP. Computer models of watershed hydrology. Computer models of watershed hydrology, 1995. xiv + 1130 p.
[43] Singh VP, Frevert D. Mathematical models of small watershed hydrology and applications. Mathematical models of small watershed hydrology and applications, 2002. xxi + 950 p.
[44] Taylor P, Fahrig L, With KA. Connectivity conservation. Cambridge University Press, 2006. p. 29–44 [Ch. Landscape connectivity: back to the basics].
[45] Taylor PD, Fahrig L, Henein K, Merriam G. Connectivity is a vital element of landscape structure. Oikos 1993;68(3):571–3.
[46] Tischendorf L, Fahring L. On the usage and measurement of landscape connectivity. Oikos 2000;90(1):7–19.
[47] Vidal Vazquez E, Vivas Miranda JG, Paz Gonzalez A. Characterizing anisotropy and heterogeneity of soil surface microtopography using fractal models. Ecol Modell 2005;182:337–53.
[48] Vogel HJ. A numerical experiment on pore size, pore connectivity, water retention, permeability, and solute transport using network models. Eur J Soil Sci 2000;51(1):99–105.
[49] Vogel HJ, Roth K. Quantitative morphology and network representation of soil pore structure. Adv Water Resour 2001;24(3–4):233–42.
[50] Western AW, Bloschl G, Grayson RB. How well do indicator variograms capture the spatial connectivity of soil moisture? Hydrol Process 1998;12:1851–68.
[51] Western AW, Bloschl G, Grayson RB. Toward capturing hydrologically significant connectivity in spatial patterns. Water Resour Res 2001;37(1):83–97.
[52] Xu C, Dowd PA, Mardia KV, Fowell RJ. A connectivity index for discrete fracture networks. Math Geol 2006;38(5):611–34.
[53] Zinn B, Harvey CF. When good statistical models of aquifer heterogeneity go bad: a comparison of flow, dispersion, and mass transfer in connected and multivariate Gaussian hydraulic conductivity fields. Water Resour Res 2003;39(3):1051.